Hindawi
Journal of Nanomaterials
Volume 2019, Article ID 6808530, 14 pages
https://doi.org/10.1155/2019/6808530

Research Article

Physical Absorption of Folic Acid and Chitosan on Dihydroartemisinin-Loaded Poly-Lactic-Co-Glycolic Acid Nanoparticles via Electrostatic Interaction for Their Enhanced Uptake and Anticancer Effect

Chien Ngoc Nguyen,[1,2] **Bao Ngoc Tran**,[1] **Hoa Nguyen Thi**,[3] **Phong Pham Huu**,[4] **and Huong Nguyen Thi**[5]

[1]*Department of Pharmaceutical Industry, Hanoi University of Pharmacy, Hanoi, Vietnam*
[2]*National Institute of Pharmaceutical Technology, Hanoi University of Pharmacy, Hanoi, Vietnam*
[3]*K68 Student, Hanoi University of Pharmacy, Hanoi, Vietnam*
[4]*Department of Pharmaceutics, Hai Duong Central College of Pharmacy, Hai Duong, Vietnam*
[5]*Rectorial Board, Hai Duong Central College of Pharmacy, Hai Duong, Vietnam*

Correspondence should be addressed to Chien Ngoc Nguyen; nguyenngocchien@yahoo.com

Received 31 January 2019; Accepted 22 May 2019; Published 13 June 2019

Academic Editor: Oscar Perales-Pérez

In this study, dihydroartemisinin (DAR), an anticancer agent with low toxicity, was loaded into poly-lactic-co-glycolic acid (PLGA) nanoparticles. The obtained PLGA cores were then coated with chitosan (CS) and/or folic acid (FA) by electrostatic interactions to enhance their anticancer and cellular uptake properties. DAR-loaded PLGA nanoparticles were prepared by the solvent evaporation method. CS and FA solutions at different ratios were dispersed concurrently into the PLGA suspension to facilitate electrostatic interactions and form nanosuspensions. The physiochemical properties of nanoparticles such as average particle size (Z), polydispersity index (PDI), zeta potential (ZP), TEM image, X-ray diffraction, and encapsulation efficiency were determined. We then determined the role of FA and CS coating on the nanoparticle surface in cytotoxicity, cellular uptake, and apoptosis. We show that the resultant nanoparticles were spherical and uniform, with a coating layer containing FA and CS covering PLGA cores with a Z of 223.5 ± 4.28 nm, PDI of 0.209 ± 0.03, and ZP of 15.75 ± 1.3 mV. Both FA and CS improved the cytotoxicity of nanoparticles compared to free DAR and PLGA nanoparticles in HL-60 and KB cancer cell lines. Further, FA enhanced the cellular uptake of nanoparticles to a greater extent than CS. However, CS contributed more to apoptosis induction than FA.

1. Introduction

Dihydroartemisinin (DAR) is an artemisinin derivative that is primarily used in the treatment of malaria. Recent studies have demonstrated that artemisinin and its derivatives have anticancer properties with low toxicity [1, 2]. Particularly, DAR has demonstrated significant cytotoxicity to osteosarcoma, pancreatic cancer, and ovarian cancer cells [3–5]. One of the most important mechanisms of DAR is generating free radicals through homogenous division of the weak endoperoxide bridge (RO-OR), in the form of hydroperoxide or hydroxyl radical based on Fenton reaction. However, these free radicals might contribute to a reduction in the stability of DAR in aqueous solution. One option is to entrap the drug into nanoparticle (NP) cores or nanocapsule reservoirs to store DAR during pharmaceutical industry processing and circulation throughout the body [6–8]. Another targeted mechanism is that by which DAR reduces cellular iron content and causes iron depletion through triggering TfR1 endocytosis, which is highly elevated in cancer than normal tissues

[9–12]. However, application of DAR in the clinic is limited by its poor pharmacokinetic profile and restriction as a monotherapy agent. In this study, the NP systems of DAR were studied to enhance its anticancer activities as well as intracellular delivery.

Poly(lactic-co-glycolic acid) (PLGA), a biodegradable polymer, has many advantages. For example, PLGA NPs show Enhanced Permeation and Retention (EPR) effect, wherein they can be diffused easily from the endothelial tissue, permeate through the vasculature, then enter into solid tumors [13, 14]. Further, PLGA is a biocompatible material, in which ester linkages are hydrolyzed in aqueous solution to release lactic acid and glycolic acid, which are then metabolized to CO_2 and H_2O and ultimately excreted from the body [15]. This PLGA platform for drug delivery is advantageous due to its minimal toxicity and approval by the FDA [13]. Furthermore, PLGA has a controlled release property, which is suitable for degradable drugs [13, 16]. Therefore, PLGA has been the center of attention for cancer therapy [17], in which, changing the surface of the PLGA-based carriers is essential to obtaining the best possible therapeutic system.

Chitosan (CS) is a natural polysaccharide comprising copolymers of $\beta(1 \rightarrow 4)$ linked glucosamine and N-acetyl glucosamine [18, 19]. With its nontoxic nature, CS has been used as a pharmaceutical excipient such as a binder in tablets or in extended release systems [20]. Due to the strong electrostatic interaction with the mucus or negatively charged mucosal surface, CS that is attached to the surface of the NP will facilitate targeting of cancer cells whose membrane is negatively charged [21–24]. Furthermore, the mucoadhesive property of CS lengthens the residence time at drug absorption sites, which leads to higher absorption and enhanced drug bioavailability [25].

Some studies have attempted to conjugate targeting agents to polymer drug carriers. For this purpose, folic acid (FA) is a popular candidate since it interacts with its related receptors. These receptors are frequently overexpressed on human cancer cells and are important for cell internalization and development. Cellular uptake of FA (vitamin B9) occurs mainly via an endocytic pathway, which is mediated by high-affinity folate receptors and cysteine-rich cell surface glycoproteins [26]. FA is essential for cellular division, especially in rapidly proliferating cancer cells. Although FA is a promising candidate, its small size as a nonantigenic ligand (MW 441.40) [27, 28] makes it difficult to locate on the surface of PLGA NPs. Several attempts have been made to chemically conjugate FA with other carriers such as PLGA, CS, or PEG [28–30]. However, there have not been any attempt to coat FA and CS concurrently on PLGA NPs for enhancement of their anticancer properties.

In this study, we developed DAR-loaded PLGA NPs, with the hypothesis that coating FA and CS on PLGA NPs will improve their uptake and anticancer properties.

2. Materials and Methods

2.1. Materials. Dihydroartemisinin (DAR) was obtained from Saokim (Hanoi, Vietnam), PLGA (Lakeshore 50 : 50 DLG 2A) was purchased from Evonik (Darmstadt, Germany), chitosan (low molecular weight, 50–190 kDa) was purchased from Sigma-Aldrich (Palo Alto, CA, USA), and folic acid (FA) was from ACROS Organics (Waltham, MA, USA). N,N′-Dicyclohexylcarbodiimide (DCC) and N-hydroxysuccinimide (NHS) were purchased from Sigma-Aldrich, CA, USA. Dichloromethane and polysorbate 80 (Tween 80) were obtained from Xilong Scientific (Shanghai, China); acetonitrile or methanol was from Merck (Darmstadt, Germany). Ellipticine and camptothecin were from Merck (KGaA, Darmstadt, Germany). All other chemicals were of reagent grade and were used without further purification.

The KB cell line and the HL-60 cell line (human acute leukemia) were originally purchased from American Type Culture Collection (ATCC) (Manassas, VA, USA). Following recovery of master stocks, cells were routinely cultured in Dulbecco's modified Eagle's medium (DMEM) (Invitrogen, Carlsbad, CA, USA) supplemented with fetal bovine serum (FBS) (Gibco Invitrogen, Grand Island, NY, USA) and 1% penicillin/streptomycin and were incubated at 37°C in a 5% CO_2 humid incubator.

2.2. Methods

2.2.1. Preparation of DAR-Loaded PLGA NPs. DAR-loaded PLGA NPs were prepared by the conventional o/w emulsion-solvent evaporation method [14, 16]. DAR and PLGA were dissolved in 5 mL dichloromethane (DCM); then, the oil phase was dispersed slowly to the external water phase (50 mL water containing Tween 80 at concentrations from 0 to 2%) with a flow rate (dropwise) of 2.5 mL per minute. The emulsion was homogenized by both sonication at 100 W using the high-intensity probe ultrasonic processor Vibra-Cell (Sonics & Materials, Newtown, CT, USA) and magnetic stirring at 1200 rpm (IKA RCT Basic IKAMAG, Germany) for 5 min in a cold ice water bath (4-5°C). The formed emulsion was then magnetically stirred continuously for 3 h to evaporate DCM. The obtained nanosuspension and free drugs were washed 3 times by ultrafiltration (10 kDa, Millipore, Billerica, MA, USA) to obtain the final suspension of PLGA NPs.

2.2.2. Adsorption of CS and FA onto PLGA NPs

(1) Preparation of CS-Coated PLGA NPs (CS-PLGA NPs). CS were coated onto PLGA NPs by physically electrostatic interactions [8]. Briefly, the solution of CS in acid acetic 1% was added to the suspension of DAR-loaded PLGA NPs. After stirring for 30 min (1000 rpm), the CS-coated NPs were recovered by centrifugation with ultrafiltration (CS-PLGA nanoparticles).

(2) Preparation of PLGA NPs Coated with CS and FA (FA/CS Physical NPs). The FA solution in 0.4 M aqueous sodium hydroxide (pH 7.4) and CS solution were added concurrently to the suspension of DAR-loaded PLGA NPs and stirred for 1.5 h. The obtained CS- and FA-coated NPs were then recovered by centrifugation with ultrafiltration.

(3) Preparation of PLGA NPs Coated with FA/CS Chemical Conjugate (FA/CS Chemical NPs) (for Comparison Purpose). FA/CS conjugated polymer was synthesized based on a carbodiimide reaction [28, 31, 32]. FA, 1,3-dicyclohexylcarbodiimide (DCC), and N-hydroxysuccinimide (NHS) (molar ratio of FA : DCC : NHS = 1 : 1.2 : 1.2) were stirred in 20 mL DMSO for 12 h. The NHS-FA was obtained by crystallization into an ice-cold anhydrous ether solution containing 30% acetone. The FA/CS chemical conjugate was prepared by mixing NHS-FA with CS in DMSO (6 h, 35 ± 5°C), then centrifuging at 10000 rpm for 5 min at room temperature. The obtained precipitate was rinsed with distilled water three times and then dissolved in acetic acid solution (1%). The solution of FA/CS conjugates in acetic acid (1%) was mixed with PLGA NPs by magnetically stirring (400 rpm). The NPs were recovered by centrifugation with ultrafiltration (FA/CS chemical NPs). All experiments were protected from light.

2.2.3. Determination of Particle Size (Z) and Zeta Potential (ZP) by Dynamic Light Scattering (DLS). Particle size analysis was performed by DLS technology using Zetasizer Nano ZS90 (Malvern, Worcestershire, UK) [33, 34]. DLS yields the mean diameter (Z) and the polydispersity index (PDI), which is a measure of the width of the size distribution. The Z and PDI values were obtained at an angle of 90° in 10 mm diameter cells at 25°C. Prior to the measurements, all samples were diluted with double distilled water to produce a suitable scattering intensity.

The ZP values were determined based on environmental viscosity and Smoluchowski-Huckel's law using the Zetasizer Nano ZS90 (Malvern, Worcestershire, UK).

2.2.4. Characterization of NP Morphology. The NP samples were characterized by transmission electron microscopy (TEM) using a TEM Jeol 1210 (Jeol Ltd., Tokyo, Japan). The nanosuspension was dropped on a copper grid coated with carbon and then allowed to dry at room temperature (25 ± 5°C) before analysis.

2.2.5. Identification of Folic Acid on NPs by UV-Vis Spectroscopy. FA identification on the FA/CS physical NPs was evaluated using UV absorption spectroscopy [35]. The CS-PLGA, FA/CS physical, and FA/CS chemical NPs were dissolved in 1% acetic acid and centrifuged at 10000 rpm. The obtained supernatant was scanned in the range of 200 to 400 nm using a UV-2600 spectrophotometer (Shimadzu, Tokyo, Japan). The 1% acetic acid solution served as a blank control.

2.2.6. Analysis of In Vitro Drug Release. Drug release studies were carried out in a dialysis bag (molecular weight cutoff 10 kDa, Membrane Cell, Chicago, IL, USA) containing 3 mL of PLGA and FA/CS physical nanoparticles. The dialysis bag was placed in a 50 mL tube containing 30 mL phosphate buffer pH 6.8 (PBS) as a release medium. The tube was capped and placed on a shaking water bath rotating at 50 rpm and maintained at 37°C. At predetermined time points, 2 mL sample was collected and replaced with fresh media after sampling. The amount of DAR was measured using the Thermo-Finnigan HPLC System (San Jose, CA, USA) with an ultraviolet detector and C18 column (4.6 mm × 250 mm × 5 μm). The mobile phase was a mixture of acetonitrile and phosphate buffer solution at pH 3.0 (60 : 40, volume ratio). UV absorbance was measured at a wavelength of 210 nm with a 1.0 mL/min flow rate and 50 μL injection volume.

2.2.7. FTIR Spectroscopy. Fourier-transform infrared (FTIR) spectroscopy of pure PLGA, CS, FA, DAR, and FA/CS physical nanoparticles was performed on KBr pellets with a FTIR spectrophotometer (Spectrum Two, USA). The nanoparticle samples were lyophilized and mixed with KBr. The mixture was then pressed into thin tablets before scanning in the 400 to 4000 cm^{-1} range using the FTIR spectrophotometer.

2.2.8. X-Ray Diffraction Analysis. NP samples were lyophilized (24 h, −50 ± 5°C, 0.1 ± 0.01 mbar) before analysis. Pure DAR, PLGA, and the lyophilized powder of FA/CS physical NPs were characterized using an X-ray diffractometer (Bruker AXS D8 Advance; Bruker AXS GmbH, Karlsruhe, Germany). The X-ray powder diffractometer was conducted at 20 kV and 20 mA, using CuKa radiation (1.54 Å). The diffraction angle varied from 0° to 60° with steps of 5° per min.

2.2.9. In Vitro Cytotoxicity Assay. The colorimetric cytotoxicity assay was carried out with sulforhodamine B (SRB) dissolved in 1% acetic acid. The protein bound was determined by the optical density (OD) [36].

Sample cells were plated in 96-well plates at 1×10^{-4} cells per well density for 24 h. The cells were then treated with blank NPs, free DAR, and other NP samples (0.08, 0.4, 2.0, and 5 μg/mL) for 48 h. Ellipticine (Merck, Darmstadt, Germany) was used as the positive control of the assay. Trichloroacetic acid solution was added to the cultures and incubated at 37°C, followed by SRB incubation (30 min, 37°C). The absorbance of individual wells was analyzed at 515 nm using a microplate ELISA Plate Reader (Bio-Rad, Hercules, CA, USA). Cell viability was determined based on the following equation:

$$\text{Cell viability}\,(\%) = \frac{\left(\text{OD515}_{\text{sample}} - \text{OD515}_{\text{blank}}\right)}{\left(\text{OD515}_{\text{control}} - \text{OD515}_{\text{blank}}\right)} * 100\%. \quad (1)$$

IC50 values were calculated based on % inhibition using TableCurve 2Dv4 (System Software Inc., San Jose, CA, USA). According to the National Cancer Institute (NCI, USA), samples with IC50 less than 20 μg/mL or 5 μM were considered active.

2.2.10. Apoptosis Assay. This study was conducted using the KB cell line. Cancer cells were seeded in 6-well plates (Corning, NY, USA) at a density of 1×10^5 cells/well. DMSO was used as a negative control. The cells were washed twice with PBS and fixed with 4% paraformaldehyde at 4°C for 30 min [16, 37–39].

(1) Hoechst Staining for Nuclear Analysis. Cells were stained with Hoechst 33342 (0.5 μg/mL) for 10 min at room temperature in the dark. Thereafter, the ratio of morphologically altered cells per 400 cells was calculated under a microscope (Nikon Eclipse Ti) at excitation/emission of 350/461 nm.

(2) Caspase-3 Assay. Cells were harvested and lysed in 50 μL cell lysis buffer for 10 min and then centrifuged for 10 min (1000 rpm) to collect the cell pellet, which was then dispersed in cell lysis buffer. The obtained suspension was incubated with 50 μL 2X reaction buffer and 5 μL DEVD-pNA (200 μM) at 37°C for 1 h. The results were recorded on a microplate reader at 450 nm (TECAN, Salzburg, Austria). Caspase-3 is an important criterion to determine apoptosis mechanism for chemotherapeutic agents. This method was also mentioned in other studies [38, 39].

2.2.11. Cellular Uptake Analysis. NP samples were labeled with coumarin-6 at a concentration of 0.05 mg/mL. The uptake properties of coumarin-loaded NPs in the cancer cells (KB cell line) were characterized by flow cytometry analysis and confocal laser scanning microscopy at a density of 1×10^6 cells/well. Cells were incubated with different NPs labeled with coumarin-6 for 1 h, then harvested with trypsin and washed with PBS before analysis [8, 16, 24, 40].

(1) Flow Cytometry. The cell suspensions were analyzed for intracellular fluorescence using the NovoCyte flow cytometer followed by data analysis on the NovoExpress software (ACEA Biosciences, San Diego, CA, USA). Untreated cells were used as control samples.

(2) Confocal Laser Scanning Microscopy. Cells were then stained by Hoechst 33342 (5 μg/mL). The cover slips were then mounted on a glass slide for observation under a confocal laser scanning microscope (Axio microscope, Zeiss-Axio, Oberkochen, Germany).

2.3. Data Analysis. In each experiment, replicas were set up for the biochemical assays ($n = 6$) and for the physicochemical experiments ($n = 3$). The resulting data were analyzed using GraphPad Prism 7 (La Jolla, CA, USA). Two-way analysis of variance (ANOVA) and one-way ANOVA with Tukey's multiple comparison post hoc test were used. Data were considered statistically significant at $p < 0.05$.

3. Results

3.1. Preparation of PLGA Nanoparticles. DAR-loaded PLGA nanoparticles were prepared by the solvent evaporation emulsion technique [14, 16]. The surface of the PLGA nanoparticles was then coated concurrently with CS and FA, in which, FA was in the form of folic acid or folate (neutral molecule/deprotonated ion). The scheme illustrating the structure of the final product is shown in Figure 1.

The compositions and characteristics of the nanoparticle formulations are also shown in Table 1. DAR-loaded PLGA nanoparticles were prepared with different concentrations

Figure 1: Diagram schematizing the structure of PLGA nanoparticles coated with FA and CS.

of the drug with polymer ratios (1 : 1 to 1 : 5) and varying Tween concentrations (1.0 to 2.0%).

3.1.1. Effect of DAR : PLGA Ratios (w/w). DAR : PLGA ratios affected all PDI, Z, and ZP significantly ($p < 0.05$). However, the PDI values indicated a narrow size distribution (under 0.5, according to Malvern [34]). Z and ZP are two typical specifications to access NPs ($p < 0.05$). Therefore, all experimental formulations of PLGA NPs had acceptable values for an NP system and data analysis [33, 34].

Figure 2(a) shows that increasing the DAR : PLGA ratio from 1 : 1 to 1 : 5 led to larger average size(s) ($p < 0.05$, CT1, CT2, and CT3), in which Z was in the range of 81.8 to 137.8 nm. Higher PLGA content resulted in larger PLGA nanoparticles, which led to an increase in Z as well as absolute values of ZP. Regarding ZP, all the formulations in Figure 2(a) are in a negative range since PLGA is a polymer with uncapped end carboxyl groups [14, 17]. This property facilitated the coating process of CS (positively charged in aqueous solution) and FA (with amine functional groups) based on electrostatic interactions.

Consequently, after the screening process, CT2 (with DAR : PLGA of 1 : 3) was selected for subsequent experiments. DAR-loaded PLGA nanoparticles were also characterized with several processing inputs such as volume of outer water phase, sonification frequency, and duration of evaporation (data not shown). The final parameters were then selected as a volume ratio (oil : water) of 1 : 10, sonification power of 90 W, and the duration of solvent evaporation was 3 h.

3.1.2. Effect of Tween. Figure 2(b) illustrates the effects of Tween concentrations on Z, PDI, and ZP. First, the suspension was formed with agglomerates and big particles when Tween concentration was less than 0.5%. Second, both Z and ZP were unchanged ($p > 0.05$) when the Tween concentration increased from 1 to 1.5% (CT5 and CT6). In addition,

Table 1: Formulation composition and physiochemical characteristics for nanoparticle samples ($n = 3$).

	DAR : PLGA	Tween (%)	FA : CS (w/w)	Coating : PLGA	Z (nm)	PDI	ZP (mV)
CT1	1 : 1	1.5			81.8 ± 1.79	0.485 ± 0.04	−1.6 ± 0.68
CT2*	1 : 3	1.5			122.5 ± 2.68	0.210 ± 0.01	−10.6 ± 0.50
CT3	1 : 5	1.5			137.8 ± 0.28	0.156 ± 0.01	−13.6 ± 0.64
CT4	1 : 3	0.5			—	—	—
CT5	1 : 3	1.0			140.9 ± 5.51	0.158 ± 0.02	−17.3 ± 2.14
CT6*	1 : 3	1.5			135.7 ± 3.01	0.207 ± 0.01	−17.8 ± 0.85
CT7	1 : 3	2.0			153.2 ± 5.73	0.329 ± 0.01	−25.1 ± 2.26
CT8	1 : 3	1.0	3 : 1	0.4	—	—	—
CT9	1 : 3	1.0	2 : 1	0.4	—	—	—
CT10	1 : 3	1.0	1 : 1	0.4	223.5 ± 4.28	0.209 ± 0.03	15.75 ± 1.3
CT11	1 : 3	1.0	1 : 2	0.4	192.8 ± 1.70	0.209 ± 0.00	22.7 ± 1.06
CT12	1 : 3	1.0	1 : 3	0.4	202.9 ± 1.34	0.225 ± 0.01	24.6 ± 0.35
CT13	1 : 3	1.0	1 : 1	0.2	232.0 ± 4.50	0.219 ± 0.02	3.40 ± 1.17
CT14	1 : 3	1.0	1 : 1	0.3	215.7 ± 3.76	0.217 ± 0.01	1.7 ± 0.23
CT15	1 : 3	1.0	1 : 1	0.6	322.5 ± 2.12	0.338 ± 0.07	4.4 ± 0.16

—: precipitated or unstable; *: different in sonification frequency.

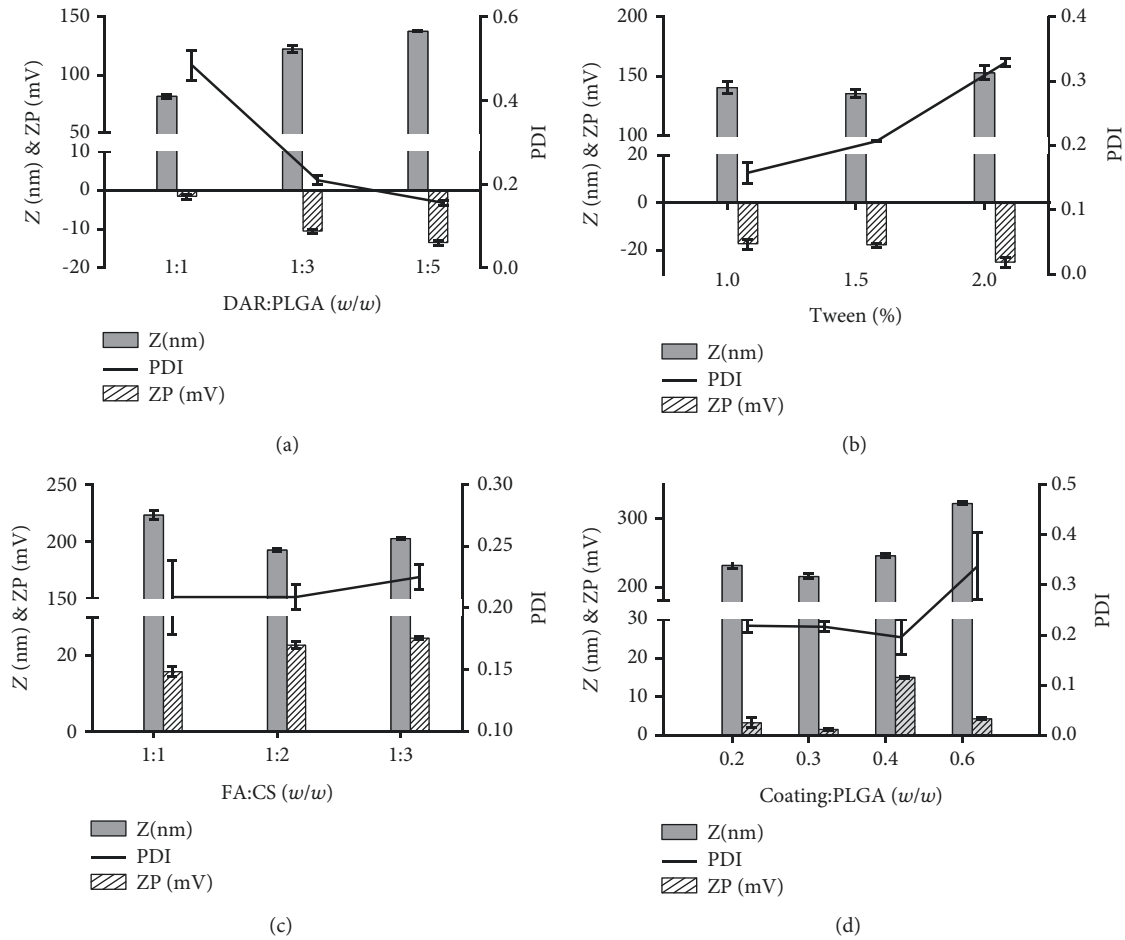

Figure 2: Effects of formulation factors on physical characteristics of nanoparticle formulation: (a) effect of DAR : PLGA ratios (w/w); (b) effect of Tween concentrations; (c) effect of FA : CS ratios (w/w); (d) effect of coating weight : PLGA ratios (w/w).

raising the Tween concentration to 2% (CT7) led to significant modification of the ZP values ($p < 0.05$). The highest Z (153.2 ± 5.7 nm) was formed at a T80 concentration of 2%. From the obtained results, the T80 concentration of 1% was chosen for further experiments.

3.2. Preparation of FA/CS onto PLGA Nanoparticles. PLGA nanoparticles of uniform size were coated based on electrostatic forces, wherein two solutions of CS and FA were dispersed concurrently into the PLGA nanosuspension. In addition to the well-known interaction of CS and PLGA, FA interacted with both CS and PLGA due to the presence of different charged functional groups of amine, carboxylic acid, and carbonyl. The more complex structure of CS located on the PLGA surface not only prevents aggregation of FA outside the nanostructure but also encapsulates FA inside.

3.2.1. Effect of FA : CS Ratios (w/w). The results of the coating processes of FA/CS on PLGA nanoparticles are presented in Table 1 and Figures 2(c) and 2(d). When FA : CS ratios were higher than 1, nanoparticle suspensions were precipitated or unstable for DLS characterization (CT8, CT9). In contrast, when the FA : CS ratio was less than 1, nanoparticles were formed. Generally, the ZP of the nanoparticle was in the positive range. Furthermore, ZP increase correlated with growing CS concentration (from 1 : 1 to 1 : 2, CT10 and CT11) ($p < 0.05$), while increasing the FA : CS ratio (from 1 : 2 to 1 : 3, CT11 and CT12) did not influence the ZP values ($p > 0.05$). Besides, the PDI values were not different significantly at varying FA : CS ratios ($p > 0.05$). The FA : CS ratio of 1 : 1 was selected for further experiments. Meanwhile, surface charge is another factor that contributes to the structure of outer colloidal layers, in which the ZP of the FA/CS layer was the same as the CS layer (positively charged).

3.2.2. Effect of Coating Weight : PLGA Ratios. A correlation between the effects of the total coating weight ratio (weight of FA and CS) and PLGA was observed. When increasing the coating weight : PLGA ratios (from 0.2 to 0.6), Z values ranged from 232 nm to over 322 nm (CT10, CT13, CT14, and CT15). Additionally, increasing the amount of coating materials caused FA to be precipitated, which interfered with the structure and stability of the whole nanoparticle system. Meanwhile, ZP values changed unpredictably when ZP was at the highest at a ratio of 0.4 (coating : PLGA, w/w; Figure 2(d)). CT10 was selected as the final formulation for further studies.

3.3. EE and LC Characteristics. All formulations, before the washing process, had an EE (%) with relatively similar values (ranging around 50%), which is lower than other reports in artemisinin derivatives [8, 16]. Specifically, DAR-loaded PLGA nanoparticles had an EE of $59.6 \pm 9.78\%$ and LC of $13.62 \pm 2.23\%$. FA/CS physical nanoparticles had an EE of 49.95 ± 2.47 and LC of $11.38 \pm 2.28\%$. This is due to the higher hydrophilic properties of DAR compared to artesunate or artemether [6]. However, after the nanosuspension was washed three times with water using ultrafiltration, all formulations had an EE (%) at over 99%. The isolation process eradicated free DAR from PLGA systems, which raised the EE (%) but reduced the LC (%) twofold.

3.4. Morphology. The morphology of PLGA NPs (Figures 3(a) and 3(b)) and FA/CS physical NPs (Figures 3(c) and 3(d)) shows that Z values reported by TEM were similar to that recorded by DLS technology. The formed nanoparticles had spherical morphology, and FA/CS-coated nanoparticles had a higher average particle size than PLGA nanoparticles. The Z increasing phenomenon was evident since CS and FA were located on the surface of PLGA nanoparticles. Interestingly, PLGA nanoparticles were observed with denser and round particles (darker and blacker), while FA/CS-coated PLGA nanoparticles had an outer grey layer (Figure 3(d)). Therefore, this finding suggests that the coating layer was not as condensed as the PLGA core.

3.5. Identification of Folic Acid on Nanoparticles by UV-Vis Spectroscopy. The appearance of FA on the nanoparticles was confirmed by UV-Vis spectroscopy analysis. The UV-Vis spectra are presented in Figure 4(a) for a sample containing FA/CS-coated nanoparticles and the corresponding FA solutions. The UV results showed an absorption band at 280 nm wavelength for the FA solution. A similar pattern for the sample containing FA/CS-coated PLGA nanoparticles confirmed that FA appeared on the PLGA surface. Meanwhile, the mentioned absorption band (280 nm) was not observed on samples containing CS, DAR, PLGA, or related nanoparticles.

3.6. In Vitro Drug Release. Figure 4(b) shows the *in vitro* drug release curves of DAR from the NPs. After 48 h, about 60% of the loaded DAR was released from uncoated PLGA NPs and 50% of DAR was released from FA/CS-coated PLGA NPs. All profiles were characterized by a first phase of rapid initial drug release followed by a second phase of slow release after 12 h. This was likely due to diffusion or erosion of the PLGA matrix during *in vitro* drug release. In particular, compared with the PLGA NPs, the FA/CS-coated NPs show a slow release pattern. Specifically, the CS layers covered the outer layers of NPs, which caused a more sustained release property. This phenomenon implies that the surface of PLGA nanoparticles were modified, which had effectively changed the location of DAR to the core of the PLGA NPs.

3.7. Fourier-Transform Infrared (FTIR) Spectroscopy Characteristics. FA/CS physical nanoparticles were characterized using FTIR spectroscopy. The comparison of the FTIR spectra of PLGA NPs and FA/CS physical NPs is shown in Figure 4(c).

The FTIR spectrum of FA (blue), the raw material, displays a broad band of NH and OH stretching vibration bands from 2800 to 3900 with characteristic peaks at 2854, 2925, 3000, 3385, and 3480 cm^{-1}. Moreover, there was a sharp peak at 1700 cm^{-1} with several minor peaks from 1000 to 1700 cm^{-1}, wherein the stretching vibration of OH phenyl was at around 1400 cm^{-1}. The amide group (CONH) appeared at 1700 cm^{-1}, and the band at 1600 cm^{-1} accounts for the bending mode vibration of amine. Particularly, only FA has the aromatic ring

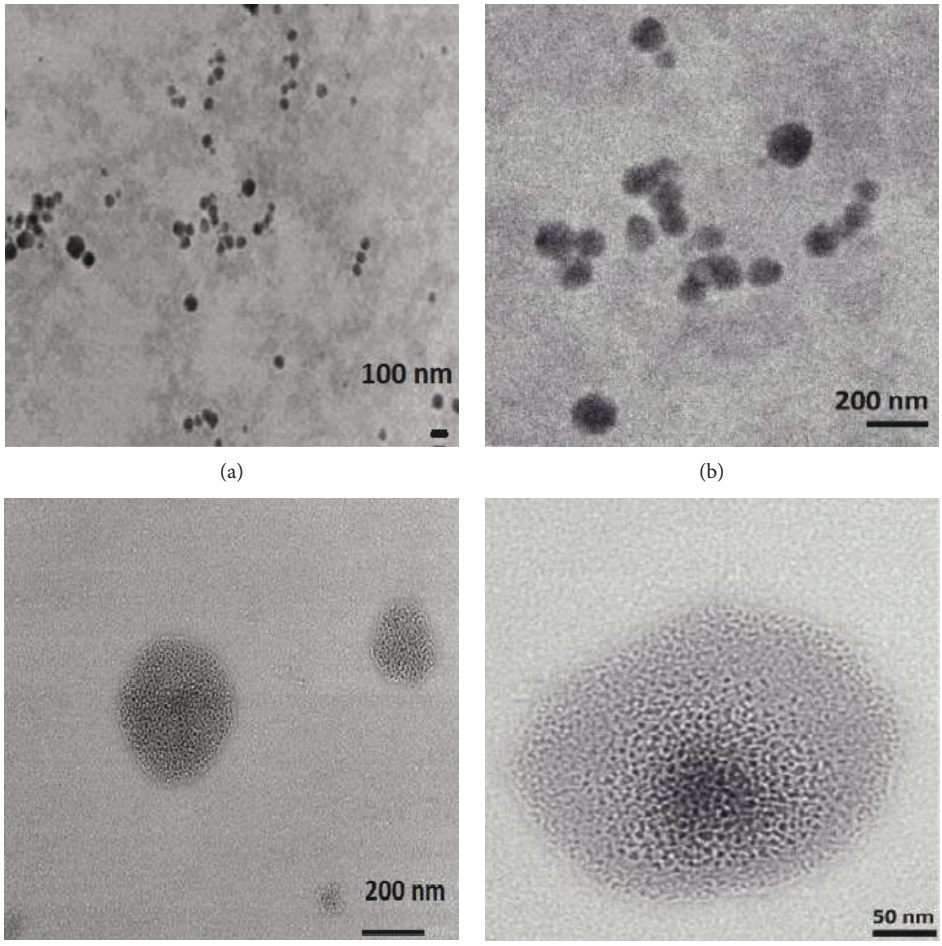

(a) (b)

(c) (d)

Figure 3: TEM images of nanoparticles: (a, b) PLGA nanoparticles and (c, d) FA/CS physical nanoparticles.

in its molecular structure. This finding was similar to several reports [28, 31].

For the FTIR of the nanoparticles, the peak and pattern of the CT10 nanoparticle were similar to those of the green spectrum (PLGA), which shows that PLGA is an important core for loading drugs and polymers. Specific peaks of FA at 1700, 1600, and 1400 cm^{-1} also appeared in the CT10 spectrum, indicating that FA was located on the PLGA surface. Additionally, peaks and patterns associated with DAR and CS also appeared in the spectrum of the PLGA formulation. Furthermore, the peak sharpness and height were not as clear as the materials, which suggested that CS and FA interacted with PLGA and DAR. Thus, some peaks of raw materials were overwhelmed in CT10. Besides, because PLGA was used at a higher concentration than others in the compositions, the peaks of other substances were subjugated by PLGA. Therefore, the finding leads to a prediction that each ingredient was constructed on PLGA cores and DAR was located inside PLGA, while CS and FA were outside.

3.8. X-Ray Diffraction Characteristics. X-ray diffraction analysis (XRD) shows that DAR and FA were in the crystallization phase, and other substances were in amorphous conditions. When preparing the nanoparticles (CT10), all substances were converted to the amorphous forms.

We observed that DAR dispersed into PLGA cores was not precipitated during experiments. On the other hand, FA was dispersed in CS outer layers at a size as small as nanoparticles or under nanoscales. The diffractogram of DAR and FA had numerous distinct reflections, indicating the crystalline nature of the drug. The reflections of DAR were observed in the range of 2° and end at 60° at a diffraction angle of 2 Theta (degree) at 7.5, 9.0, 11.0, and 12.2 (over 1000 Cps) (Figure 4(d)). Therefore, FA was observed in the range marked with 10.8, 5.2, 13.1, 16.2, and 22.8. In contrast, CS and PLGA are colloidal materials that exhibit patterns of amorphous polymers. As seen in Figure 4(d), the distinctive sharp reflections of DAR and FA disappeared in the XRD patterns of FA/CS-loaded PLGA nanoparticles.

3.9. In Vitro Cytotoxicity. In vitro cytotoxicity was determined by the MTT assay in HL-60 (negative FA receptors) and KB cells (positive FA receptors) (Figure 5) [41, 42]. Generally, blank nanoparticles were not toxic to the cells and over

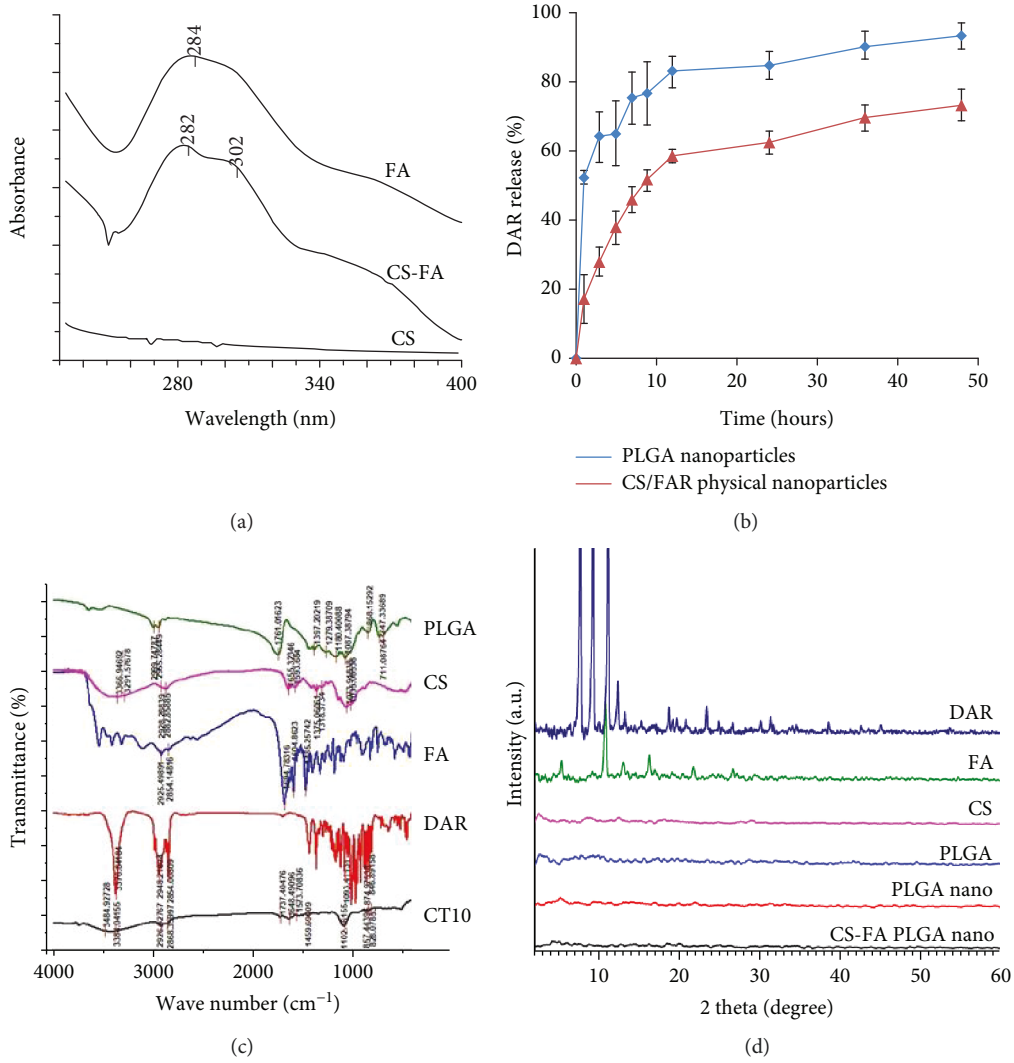

Figure 4: Physicochemical characteristics: (a) UV-VIS spectrometry, (b) *in vitro* release studies, (c) FTIR (Fourier-transform infrared) spectroscopy, and (d) X-ray diffraction (XRD).

80% of cells were viable in these studied concentrations. Specifically, all three blank nanoparticles were PLGA- and FA/CS-coated PLGA nanoparticles and CS-coated PLGA nanoparticles, in which the cell viability values were not significantly different (data not shown).

Free DAR exhibited a dose-dependent cytotoxicity, in which the IC50 for free DAR was 2.79 ± 0.07 and $2.90 \pm 0.03\,\mu$g/mL for KB and HL-60, respectively (Figure 5). Free DAR cytotoxic activity was enhanced by the PLGA preparation, which was then further increased by the CS and FA coating.

At concentrations from 0.08 to 2 μg/mL, the difference between free DAR and nanoparticle samples was also detected. Furthermore, lower cancer cell viability (under 10%) was achieved at drug concentrations of around 5 μg/mL, which indicated highly significant cytotoxicity of nanoparticle samples as well as free DAR. In addition, samples prepared by coating FA/CS or CS on the surface of PLGA NPs had higher toxicity than PLGA samples. At low concentrations, CS-coated PLGA NPs exhibited better cytotoxic activity than FA/CS-coated NPs in both cancer cell lines, while the trend was reversed at higher concentrations. Further details about the IC50 are reported in Table 2. CS-coated PLGA NPs displayed the highest *in vitro* cytotoxicity against both cancer cells, which was followed by FA/CS-coated and PLGA NPs. These findings indicate the possibility of potential applications of nanoparticle formulations for DAR in cancer treatments.

3.10. Cellular Uptake. To evaluate the cellular uptake of FA/CS-coated PLGA NPs, CS-PLGA NPs, and PLGA NPs into cells (KB cells), coumarin-6 was used to label nanoparticles at a concentration of 0.5 μg/mL for flow cytometry analysis and microscopy.

3.10.1. Flow Cytometry. After incubation for 60 min, the increasing intensity of FITC-H indicated that more NPs had permeated into the cells. Figure 6(a) confirms that all

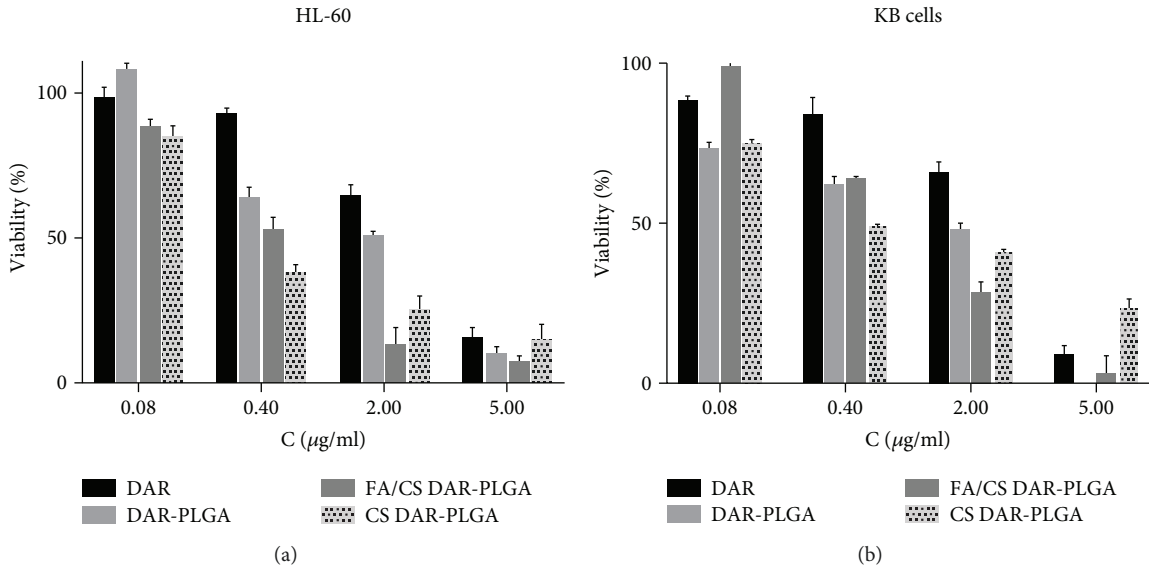

Figure 5: *In vitro* cytotoxicity of nanoparticle samples after 48 h ($n = 6$).

Table 2: Effects (IC50 μg/mL) of nanoparticle samples on cancer cell lines ($n = 6$).

No.	Samples	KB	HL-60
1	DAR (solution)	2.79 ± 0.07	2.90 ± 0.03
2	DAR-PLGA (CT6)	1.76 ± 0.09	1.85 ± 0.11
3	FA/CS physical nanoparticles (CT10)	0.37 ± 0.04	0.44 ± 0.03
4	CS-coated PLGA nanoparticles	0.24 ± 0.05	0.22 ± 0.03

FA/CS-coated PLGA NPs, CS-PLGA NPs, and PLGA NPs were taken up into the cells, compared to the negative control.

In addition, the PLGA nanoparticles showed a better uptake property (FITC-H of 10^6 to 10^7) than CS-PLGA or FA/CS chemical nanoparticles after 60 min. This might be explained by our observation that PLGA nanoparticles had the smallest particle size (around 100 nm), which facilitates uptake into cells due to passive diffusion for the first 60 min. However, FA/CS physical nanoparticles showed a similar uptake property with the PLGA nanoparticles. Interestingly, this finding suggests that FA may play a key role in improving cellular uptake into cancer cells, which have positive FA receptors.

3.10.2. Confocal Laser Scanning Microscopy (CLSM). Our confocal microscopy analysis demonstrates the internalization of nanoparticles in cells (Figure 6(b)). All the nanoparticles which were labeled green are present in the cytoplasm region with diffused distribution. The nuclei were stained blue (Hoechst), and the merged images suggest that the nanoparticles mainly distributed uniformly throughout the cytoplasm and not in the nucleus. Figure 6(b) confirms that FA/CS physical and PLGA nanoparticles are the optimal formulations for cellular uptake, which was similar to the results obtained by flow cytometry.

3.11. Apoptosis

3.11.1. Caspase-3 Assay. Figure 7(a) illustrates the caspase-3 induction activities of four samples. Generally, at concentrations of 0.08 and 0.4 μg/mL, cells underwent apoptosis by caspase activation. The descending order of samples that induced the caspase-3 synthetase was the FA/CS chemical, FA/CS physical, PLGA nanoparticles, and CS-coated PLGA nanoparticles. For a short period of time, FA/CS physical NPs and PLGA NPs showed better uptake than CS-coated PLGA samples, which caused caspase-3 to be induced more. In addition, CS-PLGA NPs were reported to release drug in a slower manner than PLGA NPs [8, 24].

This experiment showed that caspase-3 induction was at the lowest in case of using the high concentration of DAR (2 μg/mL) (compared to 0.4 or 0.08 μg/mL). As reported, DAR induces cell death by various mechanisms [3, 9] and caspase-3 pathway can be dispensable in comparison with other apoptosis pathways [43–45]. When samples were exposed to such a high concentration of DAR (2 μg/mL), all the mechanisms could occur so that the caspase-3 change was not linear. Interestingly, for FA/CS chemical nanoparticles, caspase-3 induction was concentration-dependent. This phenomenon might suggest that there may be different cell death mechanisms induced depending on the chemical complex, whether FA/CS physical, CS-coated PLGA, or PLGA nanoparticles.

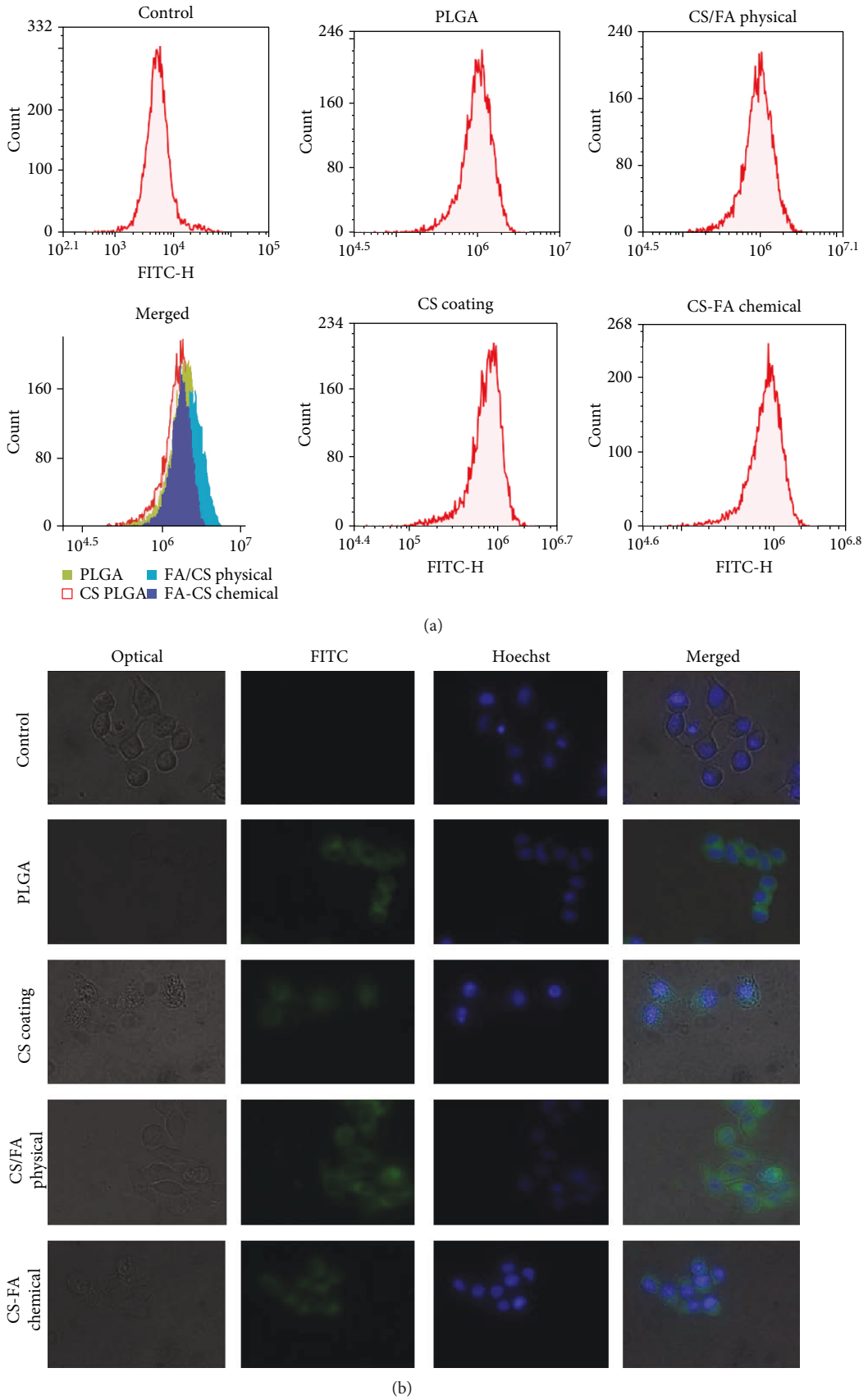

Figure 6: (a) Cellular uptake studies: flow cytometry. Line 1: negative control, PLGA nanoparticle, FA/CS electrostatically physical coating. Line 2: merged images, CS coating, FA/CS chemical complex coating. (b) Cellular uptake studies: confocal laser scanning microscopy.

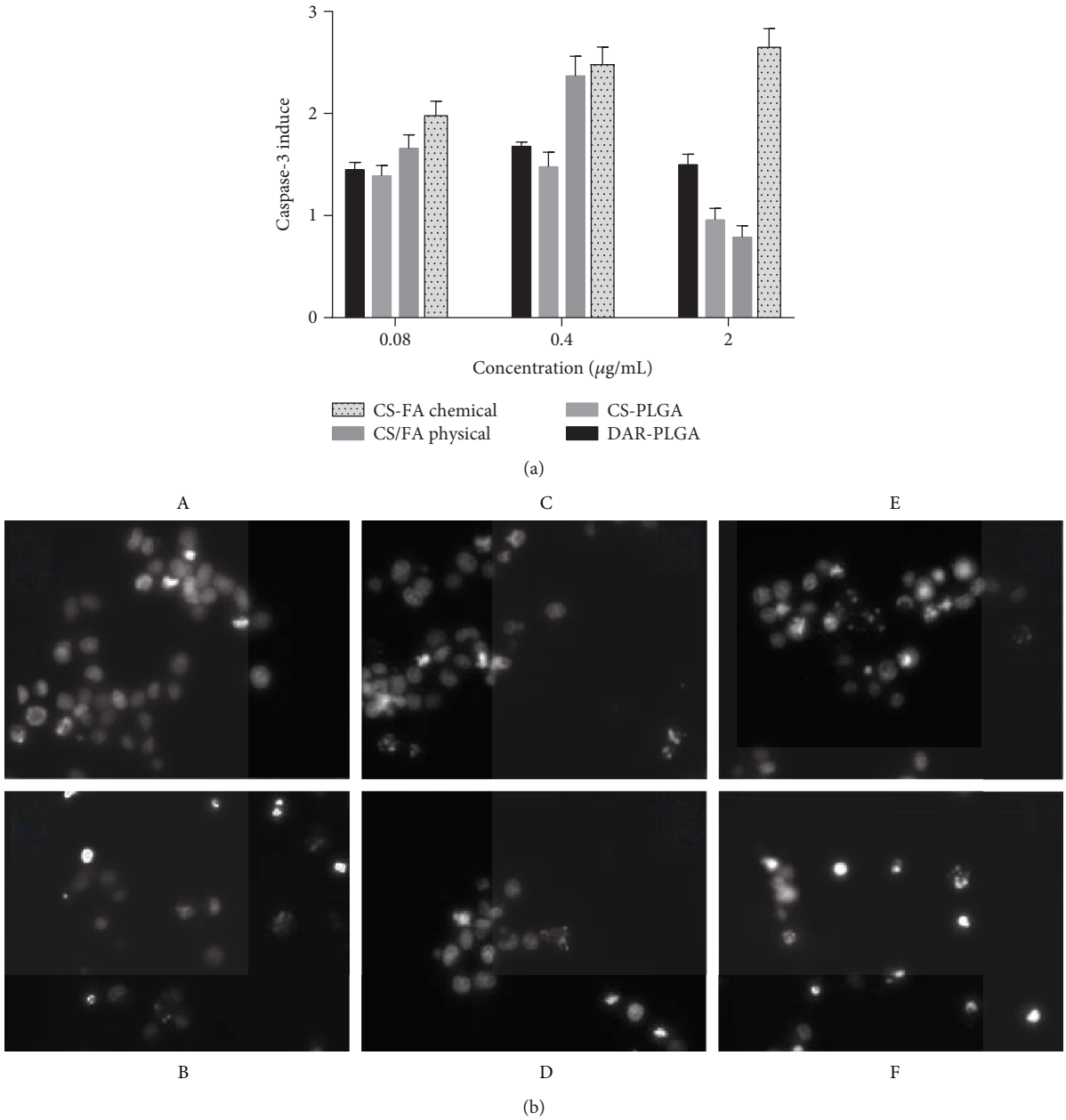

Figure 7: (a) Apoptosis studies of nanoparticle: caspase-3 induction of PLGA nanoparticles, CS-coated PLGA nanoparticles, FA/CS physical nanoparticles, and FA/CS chemical nanoparticles. (b) Apoptosis studies of nanoparticle: Hoechst staining after 1 h incubation ($n = 6$). A: negative control; B: PLGA nanoparticles; C: CS-coated PLGA nanoparticles; D: FA/CS physical nanoparticles; E: FA/CS chemical nanoparticles; F: positive control; concentrations: 2 μg/mL for samples and 5 μM for positive control.

3.11.2. Hoechst Staining for Nuclear Analysis (Figure 7(b)). In addition, the microscopy images revealed the pattern of cell death based on Hoechst staining intensity. During the apoptosis process, the cell nuclei shrink and become crescent or strip-shaped, which indicates apoptosis initiation. The transformation during apoptosis led to an increase in nuclear condensation; thus, Hoechst staining and fluorescence microscopy observation were suitable methods to observe apoptosis. Generally, after a short treatment duration (1 h), PLGA nanoparticles and all FA/CS-coated PLGA nanoparticles (physical and chemical ones) showed higher cytotoxicity than CS-coated PLGA (Table 3).

Table 3: Comparing apoptosis of nanoparticle samples for 1 h incubation.

DAR-PLGA (2 μg/mL)	CS-coated NPs (2 μg/mL)	FA/CS physical NPs (2 μg/mL)	FA/CS chemical NPs (2 μg/mL)
13.95%	10.89%	11.54%	17.98%

4. Discussion

FA has been demonstrated as an important ligand for targeted drug delivery systems for cancer treatment. Recently,

FA has been investigated as a chemical conjugate with polymer carriers such as PLGA and PEG, which can enhance drug activity [28, 29, 31]. In a different and simple approach, this study focused on the electrostatic interaction. FA and CS were coated concurrently on PLGA nanoparticles. CS has a larger and more complex structure than FA, which can provide a relatively thick layer for FA interaction. Since FA has a bipolar structure, the coating process of FA onto PLGA nanoparticles was not stable. Furthermore, FA is easier to elute from the PLGA surface compared to CS. To date, there have been no studies about coating FA onto PLGA or FA with CS in nanoparticle applications based on electrostatics. Due to the hydrophilicity of DAR, it can be dispersed into PLGA structures such that the PLGA and FA/CS layers serve as a reservoir to store DAR inside to display the controlled release property as well as improve drug stability. Furthermore, the FA/CS layer also enhances target delivery properties and anticancer activity. XRD spectrometry shows that DAR appears in an amorphous state in nanoparticles, which confirms the dispersion of DAR inside PLGA cores. TEM techniques show that FA/CS-coated PLGA nanoparticles form an outer layer covering PLGA cores.

In such an aqueous solution, FA was a dynamic molecule due to both its acidic and basic functional groups [27]. That shows that the tendency of coating FA/CS electrostatically onto PLGA nanoparticles is somewhat different from using CS or other polymers. Normally, increasing CS content increases Z values [8, 17, 40]. However, because of the flexibility of smaller molecules such as FA and the interactions of FA with the outer environment, FA fluctuates inside or on the surface of CS layers. The flexibility of FA in CS layers also explains the phenomenon observed by TEM in that the outer layer of coating was not as dense as the PLGA cores. This finding is different from other reports about the structure and morphology of CS- and FA-coated PLGA nanoparticles due to physical and chemical materials [8, 31, 35]. Finally, this formulation could take advantage of the biocompatibility of CS and PLGA and the surface activities of FA in cellular uptake, as well as the controlled release property of PLGA [13, 28, 29]. This drug delivery system (Figure 1) has not been explored for DAR in academic research or in the pharmaceutical industry. Overall, our process demonstrated here is simple enough for further industrial scale application.

All of these studied nanoformulations improved the cytotoxic activity of DAR, a natural resource substance that demonstrates anticancer activity with low toxicity to humans [4–6]. Meanwhile, CS and FA, or other excipients, did not significantly influence cell viability at relatively low concentrations (less than 5 μg/mL) (cell viability results were over 80%), which has also been confirmed by other studies [8, 35]. Consequently, it can be concluded that cytotoxic activity was mainly contributed by the drug itself and the excipients were used to improve the effects of DAR. This finding also confirmed the inhibition effect of DAR on cell proliferation in different types of cancer cell lines, which are reported by other publications [4–6].

The true nature of the KB cell line was revealed to be contaminated with HeLa cells at the time of establishment [46, 47]. This study focuses mainly on the cytotoxicity, apoptosis, and cellular uptake of NPs coated with FA (experiments were carried out on positive FA receptor cells), instead of studies on oral squamous cell carcinoma (OSCC). Thus, KB cells have been chosen due to a high expression of folic receptors [41, 42].

Furthermore, the cytotoxicity experiment in 48 h shows that CS-PLGA nanoparticles or FA/CS physical nanoparticles had higher effects compared to PLGA nanoparticles (the lower IC50, $p < 0.05$), in which CS-coated PLGA nanoparticles had the lowest IC50. This led to our conclusion that both FA and CS are effective ligands for improving the cytotoxic activity of drugs. However, CS played a better role in apoptosis enhancement. Several reports also corroborate our findings that the effect of CS was due to its chemical functions, especially when prepared in nanoparticles [8, 18, 23].

Interestingly, when preparing and comparing the function of CS and FA in nanoparticle preparation, there were new findings with regard to cellular uptake. The uptake of NPs into the cytoplasm of cells was confirmed by the fluorescence signals obtained from flow cytometry and microscopy. First, FA combined with CS (physically or chemically) enhanced the uptake of nanoparticles more than CS. The cellular uptake (by flow cytometry) and apoptosis (for a short duration) results show that FA/CS physical NPs were better than CS-coated PLGA NPs alone (CS-PLGA NPs). Figure 6(a) shows that PLGA nanoparticles and FA/CS physical nanoparticles have the highest uptake properties in KB cancer cells (positive FA receptors). While PLGA nanoparticles were the smallest particles that enhanced uptake due to passive diffusion mechanisms [14, 48], the fact that FA/CS physical nanoparticles show an equivalent property as PLGA nanoparticles confirmed the role of FA in the uptake of nanoparticles into FA-positive receptor cells. Specifically, although FA/CS physical nanoparticles and CS-coated PLGA had similar average particle size ($p > 0.05$), FA/CS physical PLGA NPs had a higher uptake property compared to CS-coated PLGA NPs. In addition, when preparing FA-CS chemical complexes, FA functional groups were also reacted and linked with the functional groups of CS. However, FA molecules that attached physically to CS layers had "more available space" to facilitate cell surface exposure. Consequently, uptake of FA/CS physical nanoparticles was better than FA/CS chemical nanoparticles for the first 60 min.

Second, when preparing the FA/CS chemical complex before coating on PLGA nanoparticles, the complex was predicted to be firmer than PLGA nanoparticles. Remarkably, cellular uptake of FA/CS chemical nanoparticles was slower than that of FA/CS physical nanoparticles. This phenomenon suggests that chemical links between CS and FA reduced the activity of FA in target delivery due to the blocking of several functional groups in both CS and FA structures. Our caspase-3 induction results also suggest that FA/CS physical NPs had a different mechanism compared to FA/CS chemical NPs as well as other FA chemical complexes coated onto PLGA nanoparticles. Previously, when cells were treated with DAR alone, the apoptosis pathway was reported to be mainly via caspase-3 [4–6]. However, preparing DAR into a nanoparticle core could change uptake properties differently (as reported) as well as the cytotoxicity (as reported in cell

viability). Meanwhile, interactions of nanoparticles or carrier polymers (PLGA, FA, and CS) with cell membranes could influence the caspase-3 results, which were assayed indirectly based on its peptide substrate (DEVD-pNA). Taken together, although there are disadvantages and advantages, this method is a new and promising approach for developing FA onto PLGA nanoparticles based on electrostatic interactions for nanoparticles in anticancer treatment (FA/CS physical nanoparticles). For further scaling-up purposes, this method is simple and reproducible.

5. Conclusion

A FA/CS physical nanoparticle was successfully prepared for DAR to enhance the *in vitro* anticancer activity of DAR and PLGA nanoparticles. This was confirmed by DLS, TEM, UV spectroscopy, FTIR spectroscopy, XRD analysis, and other *in vitro* cell experiments. The resultant nanoparticles were spherical in shape and uniform in size, with a relatively thick layer of FA/CS. FA was also confirmed to be loaded onto the surface of PLGA and inside the CS-coated layer. As predicted, drug release was more controlled and slower from FA/CS-coated PLGA NPs than from PLGA NPs. PLGA-NPs coated with FA/CS physically improved the uptake property and cytotoxic activity of nanoparticles compared to PLGA and CS-coated PLGA nanoparticles.

Data Availability

The data used to support the findings of this study are available from the corresponding author upon request.

Disclosure

This research was performed as part of the employment of the authors in Hanoi University of Pharmacy, Hanoi, Vietnam.

Conflicts of Interest

The authors declare no conflict of interest.

Acknowledgments

We would like to thank Dr. Thi Thao Do from the Institute of Biotechnology, Vietnam Academy of Science and Technology, Hanoi, Vietnam, for helping us in cytotoxicity assay and apoptosis assay.

References

[1] T. Efferth, H. Dunstan, A. Sauerbrey, H. Miyachi, and C. R. Chitambar, "The anti-malarial artesunate is also active against cancer," *International Journal of Oncology*, vol. 18, no. 4, pp. 767–773, 2001.

[2] T. Ontikatze, J. Rudner, R. Handrick, C. Belka, and V. Jendrossek, "Dihydroartemisinin is a hypoxia-active anticancer drug in colorectal carcinoma cells," *Frontiers in Oncology*, vol. 4, p. 116, 2014.

[3] H. Chen, B. Sun, S. Wang et al., "Growth inhibitory effects of dihydroartemisinin on pancreatic cancer cells: involvement of cell cycle arrest and inactivation of nuclear factor-κB," *Journal of Cancer Research and Clinical Oncology*, vol. 136, no. 6, pp. 897–903, 2010.

[4] Y. Ji, Y.-C. Zhang, L.-B. Pei, L.-L. Shi, J.-L. Yan, and X.-H. Ma, "Anti-tumor effects of dihydroartemisinin on human osteosarcoma," *Molecular and Cellular Biochemistry*, vol. 351, no. 1-2, pp. 99–108, 2011.

[5] Y. Jiao, C. M. Ge, Q. H. Meng, J. P. Cao, J. Tong, and S. J. Fan, "Dihydroartemisinin is an inhibitor of ovarian cancer cell growth," *Acta Pharmacologica Sinica*, vol. 28, no. 7, pp. 1045–1056, 2007.

[6] L. Wang, Y. Wang, X. Wang et al., "Encapsulation of low lipophilic and slightly water-soluble dihydroartemisinin in PLGA nanoparticles with phospholipid to enhance encapsulation efficiency and in vitro bioactivity," *Journal of Microencapsulation*, vol. 33, no. 1, pp. 43–52, 2016.

[7] D. Wang, J. Zhou, R. Chen et al., "Magnetically guided delivery of DHA and Fe ions for enhanced cancer therapy based on pH-responsive degradation of DHA-loaded Fe_3O_4@C@MIL-100(Fe) nanoparticles," *Biomaterials*, vol. 107, pp. 88–101, 2016.

[8] H. N. Ho, T. H. Tran, T. B. Tran, C. S. Yong, and C. N. Nguyen, "Optimization and characterization of artesunate-loaded chitosan-decorated poly(D,L-lactide-co-glycolide) acid nanoparticles," *Journal of Nanomaterials*, vol. 2015, Article ID 674175, 12 pages, 2015.

[9] Q. Ba, N. Zhou, J. Duan et al., "Dihydroartemisinin exerts its anticancer activity through depleting cellular iron via transferrin receptor-1," *PLoS One*, vol. 7, no. 8, article e42703, 2012.

[10] T. R. Daniels, T. Delgado, J. A. Rodriguez, G. Helguera, and M. L. Penichet, "The transferrin receptor part I: biology and targeting with cytotoxic antibodies for the treatment of cancer," *Clinical Immunology*, vol. 121, no. 2, pp. 144–158, 2006.

[11] S. Kasibhatla, K. A. Jessen, S. Maliartchouk et al., "A role for transferrin receptor in triggering apoptosis when targeted with gambogic acid," *Proceedings of the National Academy of Sciences*, vol. 102, no. 34, pp. 12095–12100, 2005.

[12] N. Shterman, B. Kupfer, and C. Moroz, "Comparison of transferrin receptors, iron content and isoferritin profile in normal and malignant human breast cell lines," *Pathobiology*, vol. 59, no. 1, pp. 19–25, 1991.

[13] F. Danhier, E. Ansorena, J. M. Silva, R. Coco, A. Le Breton, and V. Préat, "PLGA-based nanoparticles: an overview of biomedical applications," *Journal of Controlled Release*, vol. 161, no. 2, pp. 505–522, 2012.

[14] F. Danhier, N. Lecouturier, B. Vroman et al., "Paclitaxel-loaded PEGylated PLGA-based nanoparticles: in vitro and in vivo evaluation," *Journal of Controlled Release*, vol. 133, no. 1, pp. 11–17, 2009.

[15] A. Kumari, S. K. Yadav, and S. C. Yadav, "Biodegradable polymeric nanoparticles based drug delivery systems," *Colloids and Surfaces B: Biointerfaces*, vol. 75, no. 1, pp. 1–18, 2010.

[16] B. N. Tran, H. T. Nguyen, J. O. Kim, C. S. Yong, and C. N. Nguyen, "Developing combination of artesunate with paclitaxel loaded into poly-D,L-lactic-co-glycolic acid nanoparticle for systemic delivery to exhibit synergic chemotherapeutic response," *Drug Development and Industrial Pharmacy*, vol. 43, no. 12, pp. 1952–1962, 2017.

[17] Y. Wang, P. Li, and L. Kong, "Chitosan-modified PLGA nanoparticles with versatile surface for improved drug delivery," *AAPS PharmSciTech*, vol. 14, no. 2, pp. 585–592, 2013.

[18] D. Elieh-Ali-Komi and M. R. Hamblin, "Chitin and chitosan: production and application of versatile biomedical nanomaterials," *International Journal of Advanced Research*, vol. 4, no. 3, pp. 411–427, 2016.

[19] I. Aranaz, M. Mengibar, R. Harris et al., "Functional characterization of chitin and chitosan," *Current Chemical Biology*, vol. 3, no. 2, pp. 203–230, 2009.

[20] L. Ilium, "Chitosan and its use as a pharmaceutical excipient," *Pharmaceutical Research*, vol. 15, no. 9, pp. 1326–1331, 1998.

[21] A. Albanese, P. S. Tang, and W. C. W. Chan, "The effect of nanoparticle size, shape, and surface chemistry on biological systems," *Annual Review of Biomedical Engineering*, vol. 14, no. 1, pp. 1–16, 2012.

[22] R. Yang, W.-S. Shim, F.-D. Cui et al., "Enhanced electrostatic interaction between chitosan-modified PLGA nanoparticle and tumor," *International Journal of Pharmaceutics*, vol. 371, no. 1-2, pp. 142–147, 2009.

[23] J. N. Mehrishi, "Effect of lysine polypeptides on the surface charge of normal and cancer cells," *European Journal of Cancer*, vol. 5, no. 5, pp. 427–435, 1969.

[24] C. N. Nguyen, B. N. Tran, T. T. Do, H. Nguyen, and T. N. Nguyen, "D-optimal optimization and data-analysis comparison between a DoE software and artificial neural networks of a chitosan coating process onto PLGA nanoparticles for lung and cervical cancer treatment," *Journal of Pharmaceutical Innovation*, pp. 1–15, 2018.

[25] L. Chronopoulou, M. Massimi, M. F. Giardi et al., "Chitosan-coated PLGA nanoparticles: a sustained drug release strategy for cell cultures," *Colloids and Surfaces B: Biointerfaces*, vol. 103, pp. 310–317, 2013.

[26] AHFS, *Folic Acid*, American Society of Health-System, 2018.

[27] *The MERCK Index Online*, Royal Society of Chemistry, 2013.

[28] B. Stella, S. Arpicco, M. T. Peracchia et al., "Design of folic acid-conjugated nanoparticles for drug targeting," *Journal of Pharmaceutical Sciences*, vol. 89, no. 11, pp. 1452–1464, 2000.

[29] S.-J. Yang, F.-H. Lin, K.-C. Tsai et al., "Folic acid-conjugated chitosan nanoparticles enhanced protoporphyrin IX accumulation in colorectal cancer cells," *Bioconjugate Chemistry*, vol. 21, no. 4, pp. 679–689, 2010.

[30] H. S. Yoo and T. G. Park, "Folate receptor targeted biodegradable polymeric doxorubicin micelles," *Journal of Controlled Release*, vol. 96, no. 2, pp. 273–283, 2004.

[31] N. L. Dhas, P. P. Ige, and R. R. Kudarha, "Design, optimization and in-vitro study of folic acid conjugated-chitosan functionalized PLGA nanoparticle for delivery of bicalutamide in prostate cancer," *Powder Technology*, vol. 283, pp. 234–245, 2015.

[32] Y. Zu, Q. Zhao, X. Zhao, S. Zu, and L. Meng, "Process optimization for the preparation of oligomycin-loaded folate-conjugated chitosan nanoparticles as a tumor-targeted drug delivery system using a two-level factorial design method," *International Journal of Nanomedicine*, vol. 6, pp. 3429–3441, 2011.

[33] Malvern Instruments, "Dynamic light scattering: an introduction in 30 minutes," Technical Note MRK656-01, Malvern Instruments Ltd., 2012.

[34] Malvern_Instruments, *Zetasizer Nano Series User Manual*, Malvern Instruments Ltd., Worcestershire, UK, 2004.

[35] C. Santos, P. Gomes, J. A. Duarte, M. M. Almeida, M. E. V. Costa, and M. H. Fernandes, "Development of hydroxyapatite nanoparticles loaded with folic acid to induce osteoblastic differentiation," *International Journal of Pharmaceutics*, vol. 516, no. 1-2, pp. 185–195, 2017.

[36] P. Skehan, R. Storeng, D. Scudiero et al., "New colorimetric cytotoxicity assay for anticancer-drug screening," *JNCI Journal of the National Cancer Institute*, vol. 82, no. 13, pp. 1107–1112, 1990.

[37] E.-J. Park, J. Yi, K.-H. Chung, D.-Y. Ryu, J. Choi, and K. Park, "Oxidative stress and apoptosis induced by titanium dioxide nanoparticles in cultured BEAS-2B cells," *Toxicology Letters*, vol. 180, no. 3, pp. 222–229, 2008.

[38] H. Oyaizu, Y. Adachi, S. Taketani, R. Tokunaga, S. Fukuhara, and S. Ikehara, "A crucial role of caspase 3 and caspase 8 in paclitaxel-induced apoptosis," *Molecular Cell Biology Research Communications*, vol. 2, no. 1, pp. 36–41, 1999.

[39] Y.-Y. Lu, T.-S. Chen, J.-L. Qu, W.-L. Pan, L. Sun, and X.-B. Wei, "Dihydroartemisinin (DHA) induces caspase-3-dependent apoptosis in human lung adenocarcinoma ASTC-a-1 cells," *Journal of Biomedical Science*, vol. 16, no. 1, p. 16, 2009.

[40] B. N. Tran, H. T. Nguyen, J. O. Kim, C. S. Yong, and C. N. Nguyen, "Combination of a chemopreventive agent and paclitaxel in CD44-targeted hybrid nanoparticles for breast cancer treatment," *Archives of Pharmacal Research*, vol. 40, no. 12, pp. 1420–1432, 2017.

[41] K. Siwowska, R. M. Schmid, S. Cohrs, R. Schibli, and C. Müller, "Folate receptor-positive gynecological cancer cells: in vitro and in vivo characterization," *Pharmaceuticals*, vol. 10, no. 4, p. 72, 2017.

[42] S. D. Weitman, R. H. Lark, L. R. Coney et al., "Distribution of the folate receptor GP38 in normal and malignant cell lines and tissues," *Cancer Research*, vol. 52, no. 12, pp. 3396–3401, 1992.

[43] R. U. Jänicke, P. Ng, M. L. Sprengart, and A. G. Porter, "Caspase-3 is required for α-fodrin cleavage but dispensable for cleavage of other death substrates in apoptosis," *Journal of Biological Chemistry*, vol. 273, no. 25, pp. 15540–15545, 1998.

[44] T. S. Zheng, S. Hunot, K. Kuida et al., "Deficiency in caspase-9 or caspase-3 induces compensatory caspase activation," *Nature Medicine*, vol. 6, no. 11, pp. 1241–1247, 2000.

[45] G. Kroemer, L. Galluzzi, P. Vandenabeele et al., "Classification of cell death: recommendations of the Nomenclature Committee on Cell Death 2009," *Cell Death and Differentiation*, vol. 16, no. 1, pp. 3–11, 2009.

[46] L. Jiang, X. Zeng, Z. Wang, and Q. Chen, "Cell line cross-contamination: KB is not an oral squamous cell carcinoma cell line," *European Journal of Oral Sciences*, vol. 117, no. 1, pp. 90-91, 2009.

[47] L. Vaughan, W. Glänzel, C. Korch, and A. Capes-Davis, "Widespread use of misidentified cell line KB (HeLa): incorrect attribution and its impact revealed through mining the scientific literature," *Cancer Research*, vol. 77, no. 11, pp. 2784–2788, 2017.

[48] J. Panyam and V. Labhasetwar, "Dynamics of endocytosis and exocytosis of poly(D,L-lactide-*co*-glycolide) nanoparticles in vascular smooth muscle cells," *Pharmaceutical Research*, vol. 20, no. 2, pp. 212–220, 2003.